J Mater Sci: Mater Med (2007) 18:417–427
DOI 10.1007/s10856-007-2000-6

Performance of laser bonded glass/polyimide microjoints in cerebrospinal fluid

A. Mian · G. Newaz · D. G. Georgiev · N. Rahman · L. Vendra · G. Auner · R. Witte · H. Herfurth

Received: 20 October 2004 / Accepted: 24 October 2005

Abstract In this paper, laser bonded microjoints between glass and polyimide is considered to examine their potential applicability in encapsulating neural implants. To facilitate bonding between polyimide and glass, a thin titanium film with a thickness of 2 μm was deposited on borosilicate glass plates by a physical vapor deposition (PVD) process. Titanium coated glass was then joined with polyimide by using a cw fiber laser emitting at a wavelength of 1.1 μm (1.0 W) to prepare several tensile samples. Some of the samples were exposed to artificial cerebrospinal fluid (aCSF) at 37°C for two weeks to assess long-term integrity of the joints. Both the as-received and aCSF soaked samples were subjected to uniaxial tensile loads for bond strengths measurements. The bond strengths for the as-received and aCSF soaked samples were measured to be 7.31 and 5.33 N/mm, respectively. Although the long-term exposure of the microjoints to aCSF has resulted in 26% reduction of bond strength, the samples still retain considerably high strength as compared with the titanium-polyimide samples. The failed glass/polyimide samples were also analyzed using optical microscopy, and failure mechanisms are discussed. In addition, a two dimensional finite element analysis (FEA) was conducted to understand the stress distribution within the substrate materials while the samples are in tension. The FEA results match reasonably well with the experimental load-displacement curves for as-received samples. Detailed discussion on various stress contours is presented in the paper, and the failure mechanisms observed from the experiment are shown in good agreement with the FEA predicted ones.

A. Mian (✉)
Department of Mechanical and Industrial Eng., Montana State University, Bozeman, MT 59717
e-mail: amian@me.montana.edu

N. Rahman · L. Vendra
Department of Mechanical Engineering, Wayne State University Detroit, Michigan, USA

G. Newaz
Department of Mechanical Engineering; Center for Smart Sensors and Integrated Microsystems (SSIM); Institute for Manufacturing Research, Wayne State University Detroit, Michigan, USA

D. G. Georgiev · G. Auner
Center for Smart Sensors and Integrated Microsystems (SSIM), Wayne State University Detroit, Michigan, USA

R. Witte · H. Herfurth
Center for Laser Technology, Fraunhofer USA, Plymouth, Michigan, USA

Introduction

Advanced micro-technologies offer new opportunities for the development of active biological implants that are often used to restore malfunctioned physiological systems. For example, the cardiac and hearing disorders are currently treated by using pacemakers [1] and cochlear implants [2–6], respectively. The implantable drug delivery systems are employed to locally effuse chemicals and drugs such as pain medication, hormones and other pharmaceutical compounds [7–9]. In addition, these systems can also be programmed to monitor health status and provide therapeutic treatment *in situ* [10]. Implantable devices are being developed for providing electrical stimulations to minimize progressive atrophy and weakness that occur in denervated muscles [11–13]. Peachy et al. [14] and Chow et al. [15] showed that the damaged photoreceptor cells (fail to send electrical signals to the rest of the eye and eventually to the brain) that result in blindness can be replaced by the subretinal implant devices. The study of Humayun et al. [16] has showed successful results to restore vision by permanently implanting a retinal

prosthesis in the blind eye. Besides, many researchers [17–20] have focused their attentions in neural implants due to the growing concerns of various neurodegenerative diseases. For example, multiple sclerosis, as well as spinal cord injuries may cause the loss of synaptic input at neuromuscular junctions and, consequently, of voluntary motor control [21]. Most of the neural implants aim to contact the nervous system with prosthetic devices in order to supplement or substitute the hampered functions of the nervous systems. The implantation devices, neural implants in particular, need to be packaged with materials that do not degrade when exposed to a biological environment such as the one in the brain. In addition, the encapsulation materials need to have a biocompatible tissue interface with the body. Various materials such as titanium, glass and specific ceramics have been extensively tested for their biocompatibility and are currently being used for electronics housing in pacemakers. Flexible structures like electrode wires and lead-outs are insulated and covered with proven biocompatible materials such as silicone rubber PDMS (Poly (Dimethyl Siloxane)), polyurethane and other polymer materials (e.g. polyimide) [22].

Often similar or dissimilar encapsulation materials need to be joined together to provide hermetic packaging of the implant microelectronics. The joining methods must not utilize or give rise to any third material, which is not biocompatible. Today, adhesives and soldering are widely used to join dissimilar materials, however often they are not biocompatible and possess poor long-term stability. Also, these methods are not always capable of generating micron size bonds that are necessary for encapsulating the miniature implant systems. In addition, high heat input of soldering and the material shrinkage during curing of adhesives makes precision alignment difficult and automation very challenging. Proven methods for adhesive-free localized joining and hermetic sealing of non-metals and dissimilar material combinations in particular, do not yet exist for implantable microsystems. Laser micromachining procedures that provide focusing capabilities to spot sizes in the micrometer range can overcome all of the limitations posed by the adhesive or soldering bonds. In this method, the laser energy can be controlled precisely in the focal spot enabling a very localized materials processing with minimum heat effect on the overall part.

Proven biocompatible materials such as glass, titanium, and polyimide are potential candidates in encapsulating devices for neural implants. In this study, titanium coated borosilicate glass and polyimide sheet were joined using a transmission type laser-joining procedure. Few of the samples were soaked in artificial cerebrospinal fluid (aCSF) solution for two weeks at 37°C to understand the long-term stability of the bond. Both the aCSF soaked and as-received bi-material systems were subjected to tensile loading using a microtester, and failure loads per unit bond length were documented. The failed samples were then inspected under an optical microscope, and micrographs of the surfaces near the bond areas were analyzed. A two-dimensional finite element analysis (FEA) technique was also employed to numerically understand the stress distribution in the bond area under tensile load. The FEA results provided an accurate prediction of failure initiation location and failure load when compared with the experimental results.

Laser joining technology

The laser beam with a spot size in the micron range allows the heat to be applied very precisely and defined in time and space. In contrast to the traditional joining technologies, the applicability of laser joining requires specific optical material properties. The optical properties of the materials to be joined determine the appropriate laser wavelength, as well as the laser joining technique [23–24]. The different irradiation techniques discussed in reference [23] are contour, simultaneous, quasi-simultaneous, mask, and shadow-welding that are used for joining polymers or metals. The ideal material combination includes one absorbent and one transparent part at the laser wavelength of typical industrial high power lasers such as CO_2 ($\lambda = 1064$ nm), Nd:YAG ($\lambda = 1{,}06$ nm) or diode lasers ($\lambda = 808$–980 nm). The laser energy penetrates the transparent part and is absorbed by the absorbing part, so that the heat is induced directly at the interface. This method is called 'transmission joining' [23–28], which is demonstrated in Figure 1. To generate a line bond, the circular spot of the laser energy will follow a programmed path. The transmission joining method is successfully applied in industry for plastic welding [26–28] and offers great potential for joining of dissimilar material combinations such as glass-to-silicon [23, 25] and polymer-to-metal [23–25].

Sample preparation

In our current investigation, laser irradiated bonding between glass and polyimide samples is considered. A schematic of sample geometry and size is given in Figure 2. The polyimide sheets were made of thermoplastic polyimide Imidex (Wastelake Plastic Company) and have thickness of 0.18 mm. The thickness of the borofloat® borosilicate glass substrate was 0.5 mm.

To facilitate bonding between polyimide and glass, a thin titanium film with a thickness of 2 μm was deposited on borosilicate glass plates by a physical vapor deposition process. To bond the materials, the two sides (polyimide and glass) to be bonded were pressed against each other and a laser beam was applied through the polyimide sheet. The titanium film was selected as a coupling agent because of its excellent biocompatibility and chemical reactivity suitable for such a bonding scheme. The samples were prepared by using a cw fiber laser emitting at a wavelength of

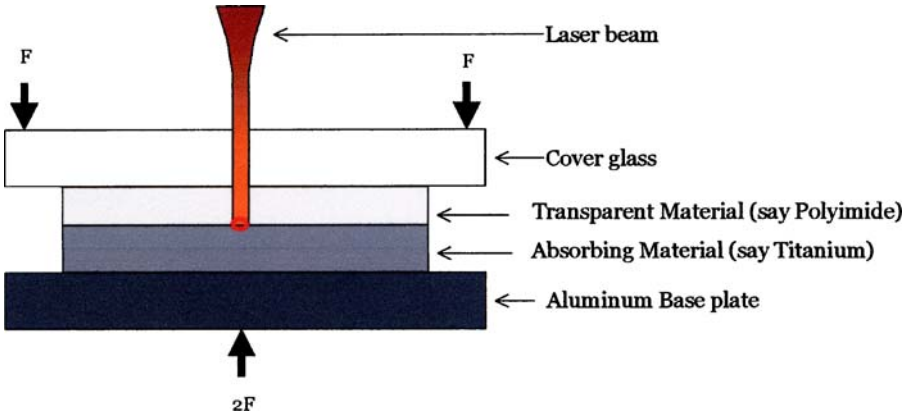

Fig. 1 Transmission joining of two materials using a laser beam.

1.1 μm (a total power of 1.0 W was used). All surfaces were carefully cleaned before the joining procedure. The laser beam was scanned at a speed of 100 mm/min along the width of the sample to generate a 6 mm long bond. In this case, a defocused fiber laser beam with a diameter of approximately 0.20 mm was applied for the experiments. Initial screening tests showed that defocusing of the beam is necessary to lower the intensity in the center of the laser spot and to avoid overheating, degeneration and burning of the polyimide that otherwise occurred even at the lowest power levels. While inspected under a microscope, the overall bond width was observed to be 0.33 mm (Figure 3). It is mentioned here that the fiber laser works in a single-mode regime producing a beam profile with a Gaussian intensity distribution.

Experimental procedure

A total of 13 samples were considered for this study. Since the bonds are targeted for use in bioencapsulation of neural implants, the effect of cerebrospinal fluid (CSF) on the bond quality needs to be investigated. In this study, the artificial cerebrospinal fluid (aCSF) from Harvard Apparatus was used. The aCSF is commonly used to mimic actual brain interstitial fluid CSF. The aCSF is identical in composition to the interstitial fluid being sampled except that it is devoid of the substances of interest (or has excess concentration of the substance to be delivered). This solution closely matches the electrolyte concentrations of CSF, which is prepared from high purity water and analytical grade reagents. It is microfiltered and sterile, and has Final Ion Concentrations (in mM): Na 150; K 3.0; Ca 1.4; Mg 0.8; P 1.0; Cl 155. Out of the prepared 13 samples, six were soaked in the aCSF solution at 37°C for two weeks.

Mechanical tensile tests

Both the seven as-received and six aCSF soaked glass/polyimide samples were tested for bond strengths

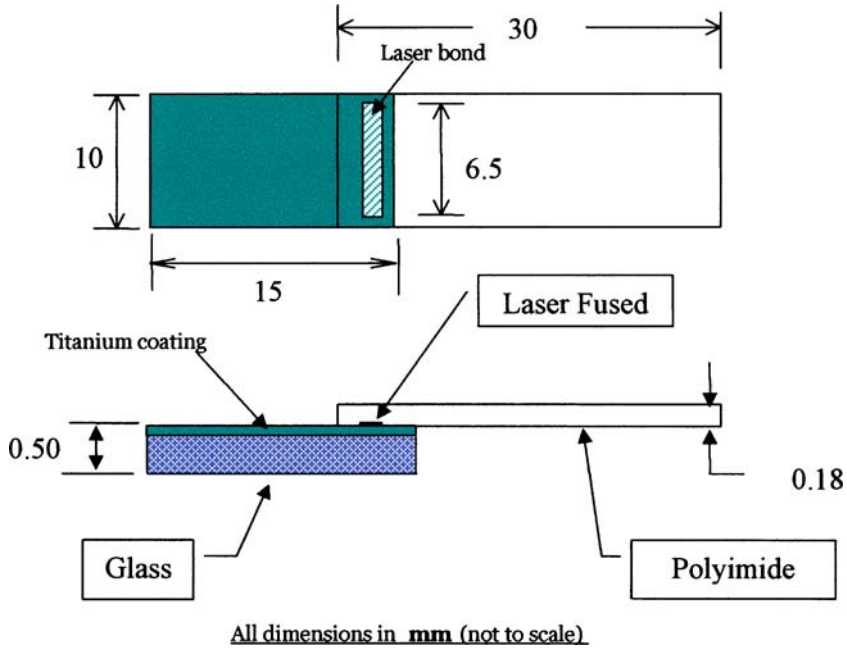

Fig. 2 Schematic of a tensile glass/polyimide sample.

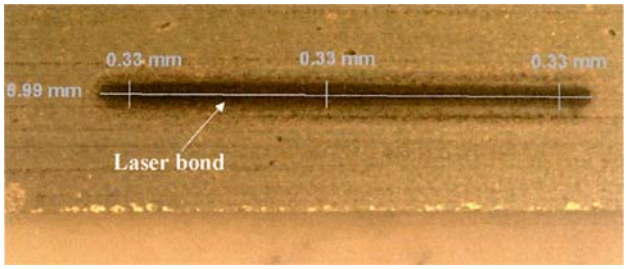

Fig. 3 An image showing the length and width of a laser bond viewed from top.

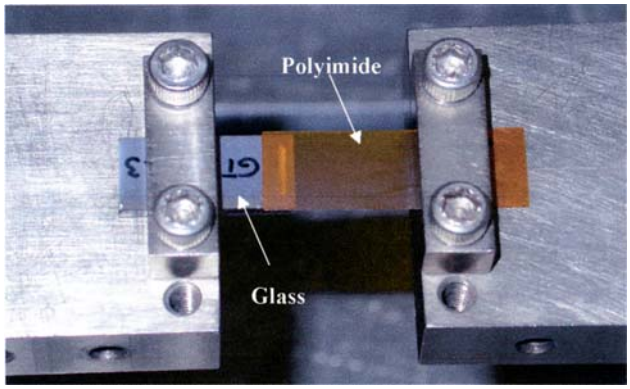

Fig. 5 Image of a sample in the test fixture.

using a microtester as shown in Figure 4. Prior to testing the aCSF soaked samples, they were wiped carefully using a water absorbent cloth and were dried at room temperature for at least 8 hours. The testing machine used in this case is called a 6-axis sub-micron tester [24, 29], which is a general-purpose micromechanical/thermal testing instrument. The machine is fully controlled by a computer, and can be operated both in displacement and load controls along six degrees of freedom, i.e., three orthogonal translations and three rotations. The displacement resolution of each closed-loop, DC-motor-drive stage is maintained at 0.1 mm in translations and 0.001 degree in rotations. A capacitance gauge installed in the equipment measures the actual displacement of a test sample.

The samples were loaded in the fixture of the testing machine as shown in Figure 5. The samples were subjected to uniaxial tension by turning on the motor that moves in the sample's length direction. The software that controls the machine also acquires load cell and capacitance gauge information (load-displacement data).

Microscopy

After the samples were tested, the failed surfaces in the bond area on both the glass and polyimide substrates were studied by using Olympus model BX 60 optical microscope with a magnification of 200×. The microstructure was investigated carefully and the images are discussed later.

Finite element analysis (FEA)

A two-dimensional finite element model for the glass/polyimide tensile samples was developed to better

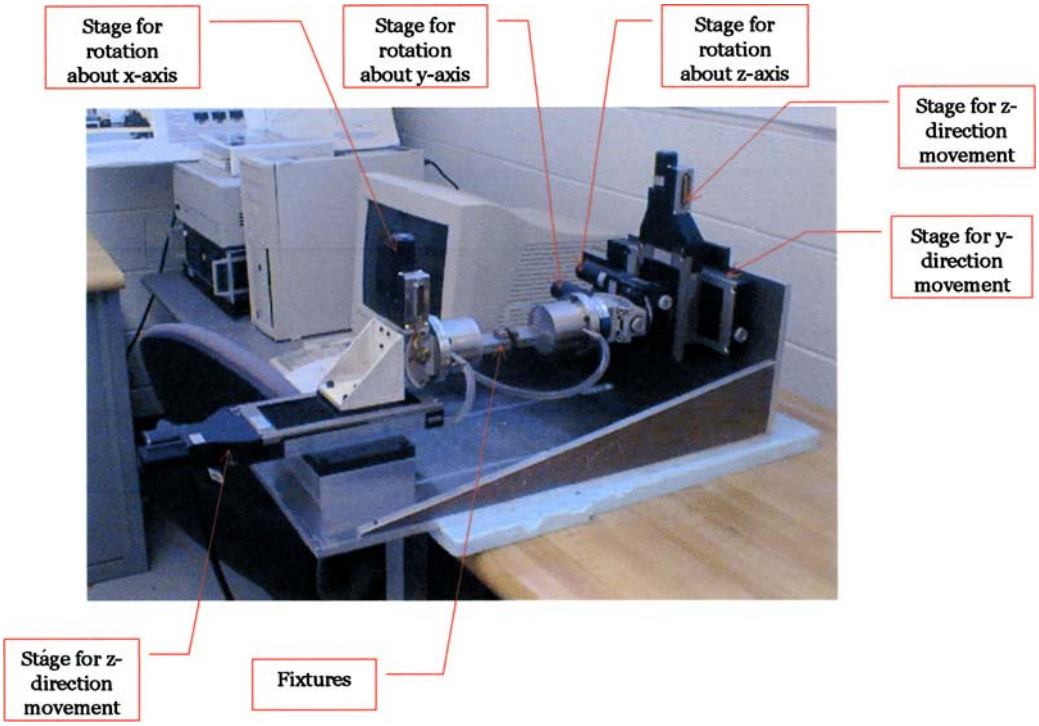

Fig. 4 6-axis microtester for tensile/fatigue tests.

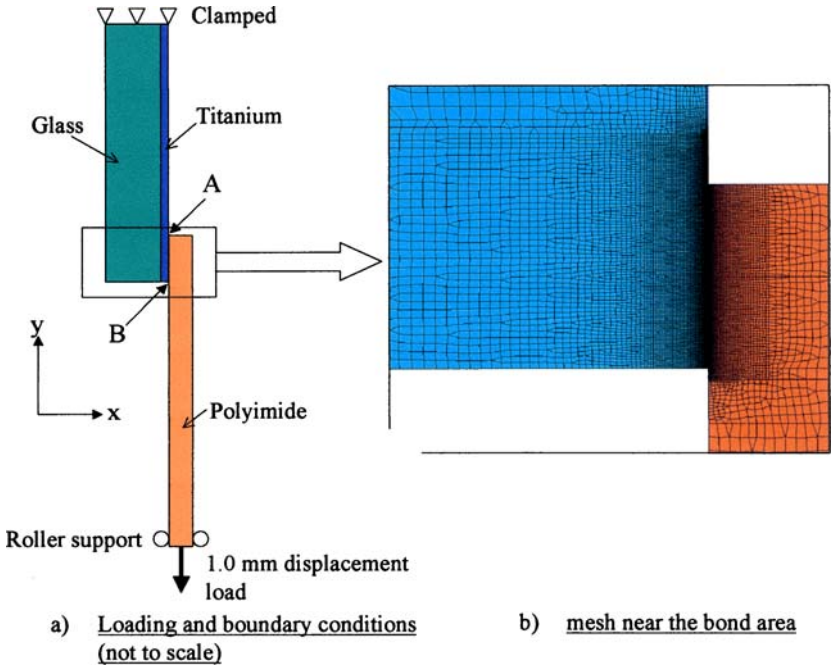

Fig. 6 Boundary Conditions and Zoomed-In Mesh view (FEA model).

understand the stress distribution within the joining area while the bi-material system was loaded in tension. The model also demonstrates the capability of FEA technique in predicting failure initiation and failure mechanism under such loading. It is mentioned here that the FEA technique has been employed to model the as-received samples where the substrate materials are considered to be strongly bonded with each other using laser processing technique.

The commercially available general purpose FEA package ABAQUS [30] was used to develop a finite element model. The joint was assumed to be a two dimensional plane-strain problem, such that only its longitudinal cross-section needed to be modeled. Hence, titanium, glass, and polyimide were modeled by using two-dimensional plane strain elements such as three-noded CPE3 and four-noded CPE4 I. Since the titanium coating is very thin (thickness of 2 μm) compared to the glass and polyimide thicknesses, and since the stress distribution within all three mating materials near the bond is crucial for analysis purposes, a very refined mesh density is adopted near the bond. The number of elements for glass, polyimide, and titanium portions were 26878, 7028, and 2591, respectively. The applied boundary and loading conditions, and mesh density near the bond are shown in Figure 6. Geometry of the model in Figure 6 represents true dimensions of the sample that was used for experiments that is given in Figure 2. However, the length of the model was equal to the gauge length between two tensile fixtures, which was 25 mm. The point where the edge of polyimide is bonded with titanium is designated as A, and the point where the edge of titanium is bonded to polyimide is designated as B (Figure 6). Thus, the bondline between titanium and polyimide in this case is AB. The length of the bondline AB was 0.33 mm as was measured under a microscope (Figure 3). In the model, the titanium-glass interface, and bondline AB between titanium and polyimide were considered to be strong. These strong bimaterial interfaces were modeled by using a common set of nodes at the glass-titanium and titanium-polyimide interfaces. The common interfacial nodes are shared by elements corresponding to both titanium and polyimide for the titanium-polyimide interface. Similarly, the common set of nodes at the glass-titanium interface is shared by the elements corresponding to the glass and titanium substrates. Effect of thickness of the very thin chemical bond created between titanium and polyimide was neglected. The applied boundary conditions were such that glass end of the joint was clamped, i.e. no movements were allowed in either the horizontal (x) or vertical (y) direction. The other (polyimide) end was restrained in the horizontal (x) direction, whereas its vertical (y-direction) nodal deflections were prescribed to be equal. A displacement of 0.12 mm was applied at the polyimide end with 20 incremental steps, and static analysis was performed. Load at every incremental step was calculated by summing up the reaction forces at the fixed end. The reaction force per unit bond length was plotted against the incremental displacement load, and was compared with the experimental load displacement curves.

Two material models such as a simple linear elastic model for glass and titanium, and a linear elastic—plastic for polyimide were used in the study. The ABAQUS standard linear-elastic material model requires two properties, namely, the modulus of elasticity and Poisson's ratio. The elastic moduli for glass and titanium were considered as 64.0 and 120.0

Table 1 Stress-strain data for polyimide used in FEA

Stress (MPa)	0	69	145	195	225	270	300	310
Strain	0	.0133	0.1	0.2	0.3	0.5	0.7	0.85

GPa, respectively, while the Poisson's ratios were assumed to be 0.2 and 0.32, respectively. The elastic-plastic model used for polyimide is also available in ABAQUS, which uses the classic von Mises yield criterion. The model requires modulus of elasticity, Poisson's ratio, and stress-strain data in the plastic region. The modulus of elasticity and Poisson's ratio for polyimide were taken to be 5.2 GPa and 0.34, respectively. The stress-strain response of polyimide in the plastic region is given in Table 1 that was used to input the plastic portion of the curve. All of the material property data were obtained from www.matweb.com. Due to the large deformation of polyimide under tension, the stiffness matrix has to be updated at each incremental applied load step. Thus, the geometric nonlinearity has to be considered by using a standard ABAQUS keyword (e.g. *loadstep, nlgeom).

Results and discussions

Experimental measurements

The microtester that is used for tensile testing poses a challenge to grip brittle materials or structures to obtain their mechanical behavior. For example, when a glass/polyimide sample is gripped for a tensile test as shown in Figure 5, it is very difficult to perform a test in tension without introducing bending moments and other undesirable forces and moments. Unfortunately, even a small bending moment could cause a brittle material to break. In addition, when the polyimide side of the sample is mounted in the micro-tester, a large preloaded compression force can be introduced to the specimen due to the deformation of the polyimide caused by the compression force of the clamps (Figure 7). However, by monitoring all 6-axis forces and moments, and releasing any unnecessary mounting forces by micropositioning the corresponding stages during or after mounting the sample, those undesirable forces/moments can be reduced to zero. The failure loads obtained for all samples were divided by the corresponding bond lengths to calculate the failure load per unit bond length. The bond lengths were measured using an optical microscope prior to testing the samples. An image showing the length of

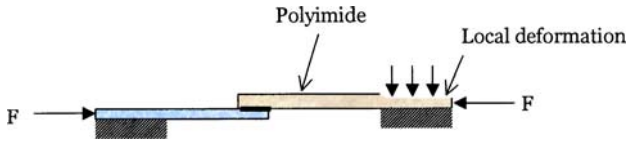

Fig. 7 Local deformation of polyimide at the grip.

Table 2 Failure loads for glass/polyimide samples

Sample type	Average bond strength (N/mm)	Std. Dev. (N/mm)
As-received samples (7*)	7.31	0.43
Samples soaked in aCSF at 37°C for 2 weeks (6*)	5.33	0.69

*Number of samples tested

a bond was presented previously in Figure 3. Test results for both the as-received and aCSF soaked samples are presented in Table 2. The average failure strength of as-received samples was observed to be 7.31 N/mm, which is more than double the bond strength of titanium/polyimide joints (3.47 N/mm) as reported in reference [24]. Out of seven samples, five broke right through the glass substrate. A representative failed sample is shown in Figure 8. Two samples separated through the bond. The failure surfaces were viewed under an optical microscope and thin titanium along with glass was observed to be broken off the glass substrate and left on the titanium surface after failure. The bond width is clear on the polyimide surface by darker zone at the center. The width is approximately 0.3 mm which is larger than the actual beam size of 0.2 mm. Possible reasons for achieving wider bond are scattering of the radiation in the polyimide film and the heat dissipation during processing. The plastic deformation of polyimide around the bond is observed, which is probably due to the Gaussian power profile of the laser beam that was used in the bonding process: only the part of the laser beam cross-section with power above a certain threshold could generate good (chemical) bonding. In short, all of the as-received samples had glass adherend failure, which implies that the bond created by laser between titanium-coated glass and polyimide is very strong. In addition, the laser process may have introduced microcracks at the titanium-glass interface that is prone to premature failure in glass substrate. The effect of laser processing parameters on the development of residual stresses is being currently studied.

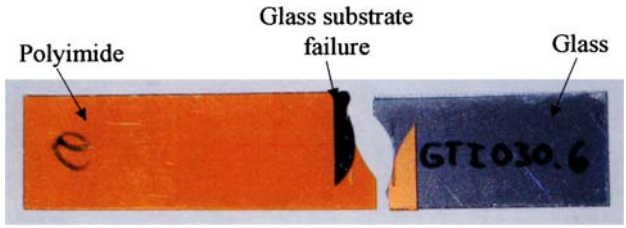

Fig. 8 A representative as-received sample showing glass substrate failure under tension.

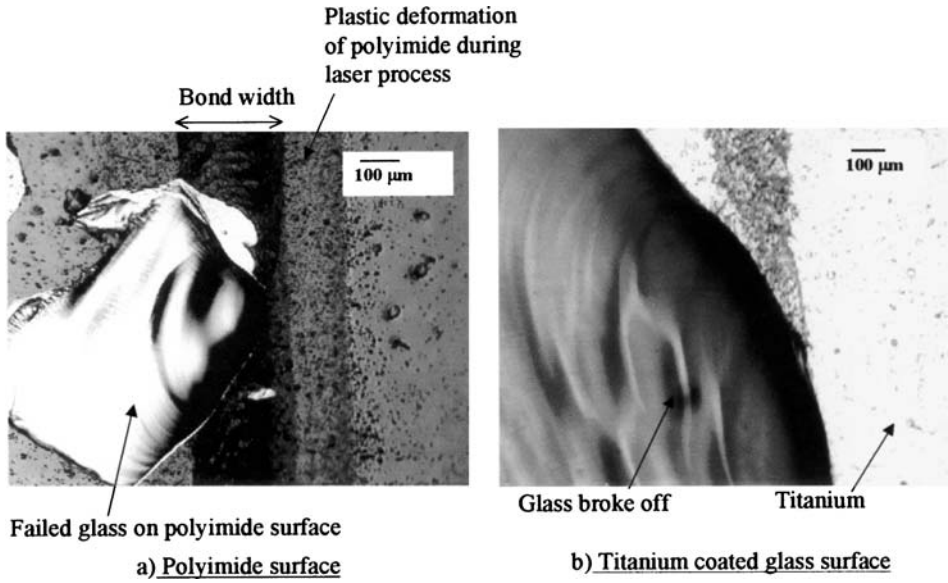

Fig. 9 Representative microscopic pictures of few of the failed as-received glass/polyimide sample (predominantly glass fracture).

The aCSF soaked samples has failure strength of 5.33 N/mm. In other words, the presence of aCSF solution has shown about 26% reduction in bond strength. However, the bond strength is still 54% higher than the titanium-polyimide bonds, and possibly has retained enough strength to be employed in bioencapsulation. Hermeticity testing of the aCSF soaked samples is underway and will be published in a future article. All of the samples are seen to fail through the interface. The failed surfaces were again studied through optical microscopy, which is shown in Figure 10. It is clear from the images in Figure 10 that the titanium/polyimide interface failure is mostly dominant in this case. As the samples are soaked in aCSF solution for a prolonged time at elevated temperature, the solution has tried to penetrate through the two sides (e.g. through points A and B shown in Figure 6 a) of the bonds that resulted in relatively weaker interfaces at the two bond edges. Moreover, titanium and glass have very low coefficients of thermal expansions (CTE) of $8.9 \times 10^{-6}/^{\circ}\text{C}$ and $3.25 \times 10^{-6}/^{\circ}\text{C}$, respectively as compared with polyimide ($55.0 \times 10^{-6}/^{\circ}\text{C}$). As the samples were heated up to the aCSF temperature of 37°C and were then cooled down to room temperature before they were tensile tested, the joint region will in fact undergo varying thermal stress due to the mismatches in CTEs of the joining materials. This stress may cause initial failure at the bond sides as they will undergo highest stresses due to the geometric and material singularities as the titanium-polyimide bimaterials are joined together. As the samples are now loaded in tension, the failure

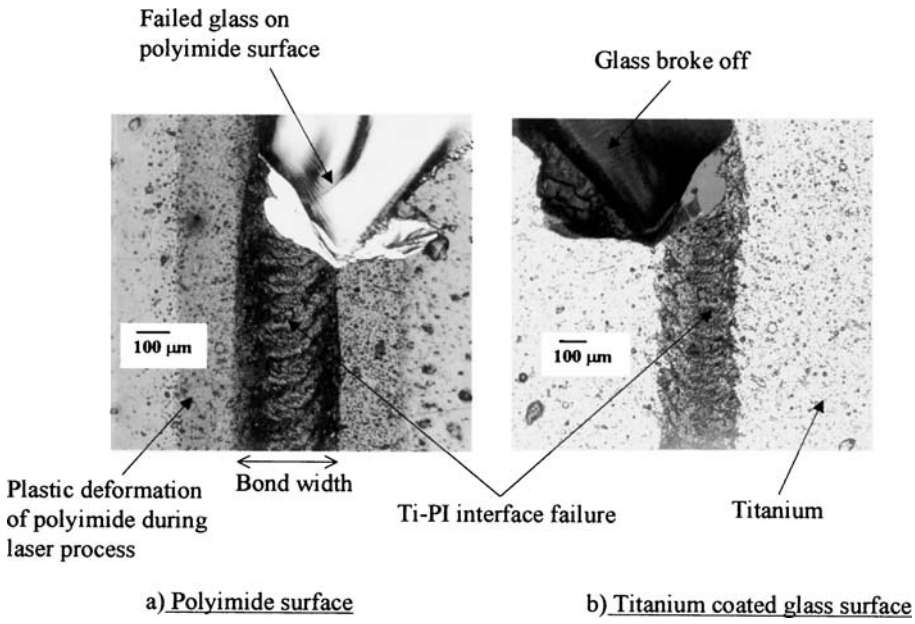

Fig. 10 Representative microscopic pictures of a failed aCSF soaked glass/polyimide sample where both interface failure and glass fracture are observed.

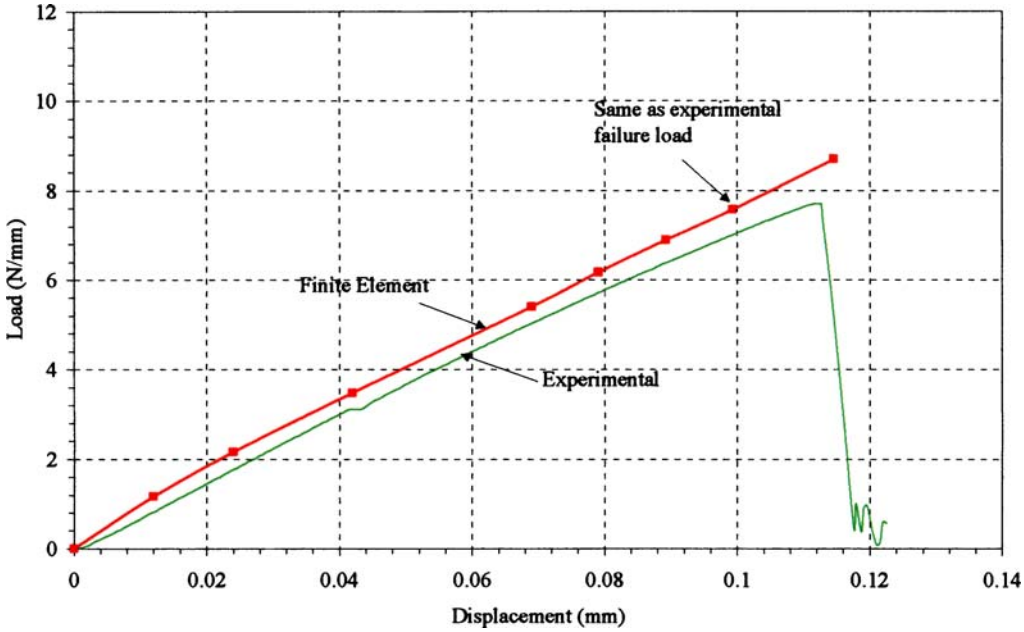

Fig. 11 Typical experimental load-displacement plots for an as-received glass/polyimide sample along with corresponding finite element data.

starts right at the weaker locations (points A or B in Figure 6a) at the titanium-polyimide interfaces and has propagated through the bondline. Thus the failure is seen to be predominantly at the titanium/polyimide interface along with some fracture of glass substrate.

Finite element analysis

Figure 11 shows the load-displacement response of the glass-polyimide sample obtained from the finite element analysis (FEA). It is mentioned in the modeling procedure that the model was developed considering strong interfaces between titanium and polyimide, and between titanium and glass. Also, it is already demonstrated in the previous paragraphs that the as-received samples possess higher bond strength than the aCSF soaked samples. In addition, the failure of glass substrate under tension clearly proves that the bonding between the mating substrates is truly high. Thus, the load displacement response from the FEA that is modeled considering strong interface between bimaterials has been compared with the experimental results for the as-received samples. From the figure, it is apparent that the FEA prediction matches reasonably well with the experimental data. However, the FEA results seem to overpredict as compared with the experimental data. The FEA prediction of the failure load of 7.3 N/mm attains at 0.1 mm displacement load as opposed to the 0.12 mm displacement as seen from the experimental data. Thus, the contour plots of various stress components discussed in the following paragraphs will be taken at the end of 0.1 mm of applied displacement load.

The deformed shape of the sample under tensile load is depicted in Figure 12. It is apparent from the figure that the substrates have rotated substantially although the system was loaded with tension in y-direction. This phenomenon is common in bimaterial joining systems due to the high differential deformations near the joint, and the amount of rotation depends on thickness and mechanical properties of the substrate materials. This rotation results in the development of all possible stress components with high stress gradients within the bond region. However, glass being very prone to flexural failure is expected to fail before the other substrates fail. From the contour plot of von Mises stress at 0.1 mm load,

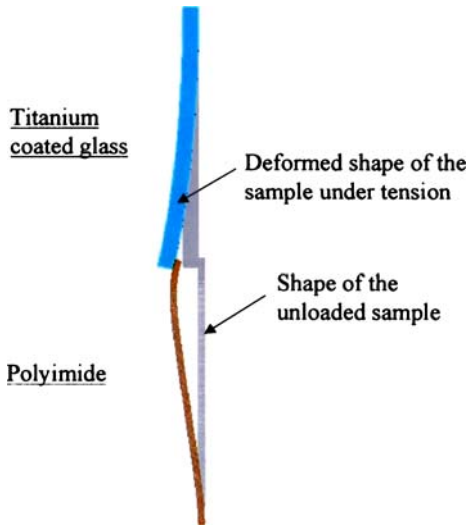

Fig. 12 Deformed shape of the glass/polyimide sample under tension (FEA results).

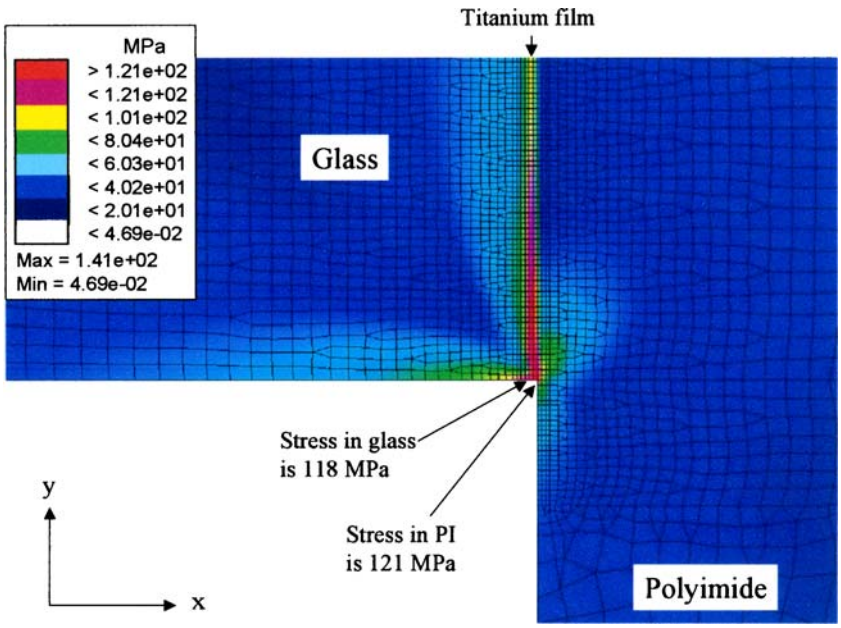

Fig. 13 Von Mises Stress distribution near location B for glass/polyimide sample under tension at 0.1 mm displacement load (FEA results).

it was observed that high stress magnitudes at the two edges (Near A and B) were attained owing to the geometric singularity and material discontinuity near the edges. However, the maximum von Mises stress was developed near the point B as shown in Figures 13. It is apparent from the figure that von Mises stresses near the point B in polyimide, glass, and titanium are 121.0, 118.0, 140.0 MPa, respectively. Thus, the stress magnitudes did not exceed the failure strengths of titanium or polyimide. Please note that the failure strength of bulk polyimide material is 130 MPa, and is assumed to be the same for 180 μm thin polyimide film. The stress magnitude of 118 MPa in glass is well below the compressive strength of glass (700 MPa for bulk glass). The stress in this region is compared with the compressive strength of glass as the compressive stress is developed due to joint rotation under tension. The attainment of high compressive stress is apparent from the x component stress contour, which is given in Figure 14. Thus, no failure is expected to start from any point near the location B. Now, the other singularity point A will be considered. As mentioned earlier, titanium and polyimide will not fail near location B where the von Mises stress was maximum. Thus titanium and polyimide near point A will also not fail. Being a very brittle material, glass can be characterized by maximum stress failure criteria. Figure 15

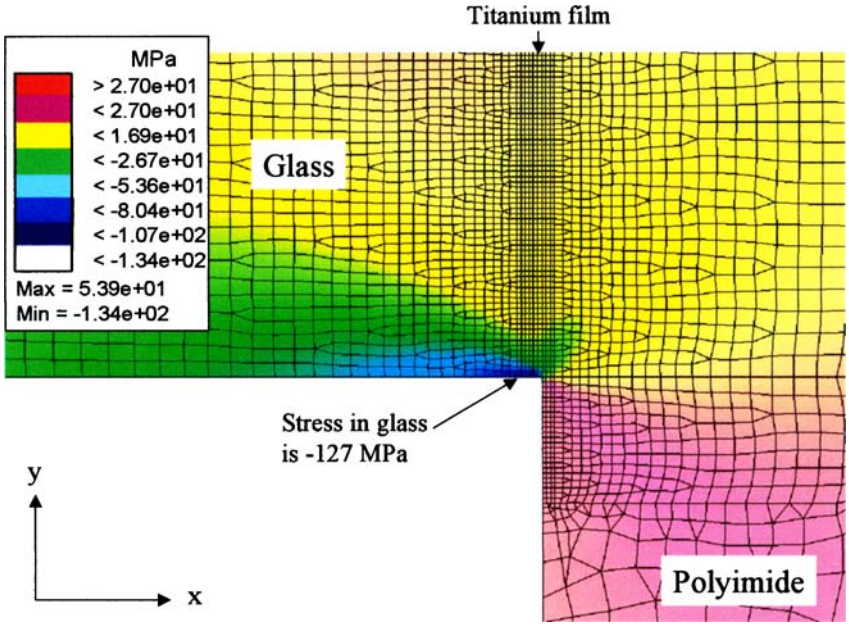

Fig. 14 x component stress distribution near the location B for glass/polyimide sample under tension at 0.1 mm displacement load (FEA results).

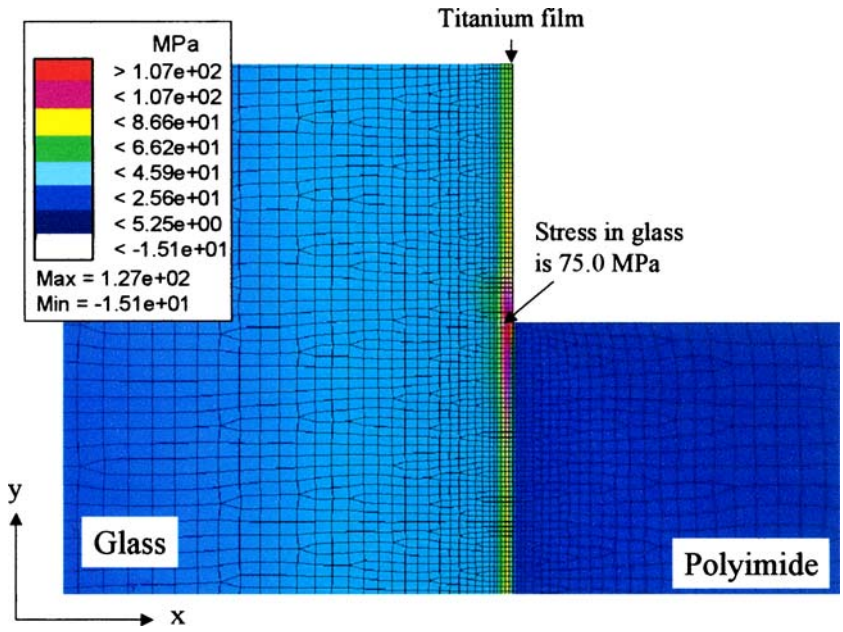

Fig. 15 y component stress distribution near the location A for glass/polyimide sample under tension at 0.1 mm displacement load (FEA results).

shows the y component stress distribution near point A. It is observed that maximum y component stress in glass is 75 MPa at the glass-titanium interface, which is higher that the tensile strength (about 70 MPa) and flexural strength (25 MPa) of glass. It is mentioned here that the bending of the glass substrate in the vicinity of point A resulted in bending stress that has contributed to additional increase in y component stress in that region. Thus the failure is expected to initiate in glass near A, and will result in partial or complete breakage of glass in the subsequent load steps. This type of failure prediction is confirmed through the microscopic images in Figure 9 where the glass failure has clearly initiated from one of the bondline ends.

Summary

In the present study, microjoint between titanium coated glass and polyimide substrates generated by transmission type laser bonding procedure is considered. A total of 13 samples were prepared. Six samples were exposed to aCSF at 37°C for two weeks. Both the seven as-received and six aCSF soaked samples were tested for bond strength using a uniaxial tensile tester. The bond strength (7.31 MPa) is double the bond strength of titanium/polyimide joints (3.47 N/mm) as reported in reference [24]. A 26% reduction (from 7.31 MPa to 5.33 MPa) in bond strength was observed due to the joints' long-term exposure to high temperature aCSF. However, the aCSF soaked samples still retain large bond strength, which is 54% higher than the reference [24] values. The failure mechanism of the as-received sample under tension was predominantly flexure type failure of the glass substrate. This is due to the rotation of the bond during tensile load as was clear from the FEA results. Prediction of the failure load from FEA model was well in agreement with the experimental results. The aCSF soaked samples failed at the titanium-polyimide bondline along with some failure of the glass substrate. The aCSF may have weakened the interfaces near the bondline edges (such as A and B) that resulted in shear type bond failure.

Acknowledgements This work was supported by the Michigan Life Sciences Corridor Grant GR-358.

References

1. K. JEFFREY, *The Implantable Defibrillator and American Health Care* (2001) 408.
2. S. MIYOSHI, T. IFUKUBE and J. MATSUSHIMA, *Transactions of the Institute of Electrical Engineers of Japan Part A*, **118-A**, no.3 (1998) 260.
3. U. MEYER-BAESE, A. MEYER-BAESE and H. SCHEICH, in Proceedings of SPIE - The International Society for Optical Engineering, **3077** (1997) 582.
4. S. ROMAN, G. CANEVET, C. LORENZI, J. TRIGLIA and C. LIEGEOIS-CHAUVEL, *Neouroreport*, **15** (4) (2004) 601.
5. J. YAO and Y. ZHANG, *IEEE Transactions on Biomedical Engineering*, **49** (2002) 1299.
6. L. T. COHEN, L. M. RICHARDSON, E. SAUNDERS and R. S. COWAN, *Hearing Research*, **179** (2003) 72.
7. J. T. SANTINI, in Proceedings of the 4th Int. Symposium on BIOMEMS, Cambridge MA, (2002).
8. R. S. SHAWGO, A. C. R. GRAYSON, Y. LI and M. J. CIMA, *Current Opinion in Solid State and Materials Science*, **6**, Issue 4 (2002) 329.
9. M. L. HANS and A. M. LOWMAN, *Current Opinion in Solid State and Materials Science*, **6**, Issue 4 (2002) 319.

10. D. LA VAN, T. MCGUIRE and R. LANGER, *Nature Biotechnology*, **21** (1) (2003) 1184.
11. S. C. NICOLAIDIS and H. B. WILLIAMS, *Microsurgery*, **21** (2001) 241.
12. R. G. DENNIS, *Medical & Biological Engineering & Computing*, **36** (1998) 225.
13. R. G. DENNIS, D. E. DOW and J. A. FAULKNE, *Medical Engineering & Physics*, **25**, Issue 3 (2003) 239.
14. N. S. PEACHEY and A. Y. CHOW, *Journal of Rehabilitation Research and Development*, **36**, No. 4 (1999) 381.
15. A. Y. CHOW and V. Y. CHOW, *Neuroscience Letters*, **225**, Issue 1 (1997) 13.
16. M. S. HUMAYUN, J. D. WEILAND, G. Y. FUJII, R. GREENBERG, R. WILLIAMSON, J. LITTLE, B. MECH, V. CIMMARUSTI, G. V. BOEMEL, G. DAGNELIE and E. D. JUAN, Jr., *Vision Research*, **43** (2003) 2573.
17. B. SCHLOSSHAUER, T. BRINKER, H. MULLER and J. MEYER, *Brain Research*, **903** (2001) 237.
18. P. R. KENNEDY and R. A. E. BAKAY, *NeuroReport*, **9** (1998) 1707.
19. K. LEE, J. HE, S. MASSIA, G. EHTESHAMI and G. RAUPP, *Journal of Micromechanics and Microengineering*, **14** (2004) 32.
20. R. J. VETTER, J. C. WILLIAMS, J. F. HETKE, E. A. NAUNAMAKER and D.R. KIPKE, *IEEE Transactions on Biomedical Engineering*, **51** (2004) 896.
21. J. W. MCDONALD, *Scientific American*, **281** (1999) 64.
22. J. MEYER, T. STIEGLITZ, O. SCHOLZ, W. HABERER and H. BEUTEL, *IEEE Transactions on Advanced Packaging*, **24** (2001) 366.
23. I. BAUER, U. A. RUSSEK, H. HERFURTH, R. WITTE, S. HEINEMANN, G. NEWAZ, A. MIAN, D. GEORGIEV and G. AUNER, *in Proceedings of SPIE—Photonics West LASE 2004: Lasers and Applications in Science and Engineering conference*, 24–29 January 2004, San Jose, California.
24. A. MIAN, G. NEWAZ, L. VENDRA, N. RAHMAN, D.G. GEORGIEV, G. AUNER, R. WITTE and H. HERFURTH, *Journal of Materials Science: Materials in Medicine*, **16** (2005) 229.
25. M. J. WILD, A. GILLNER and R. POPRAWE, *Sensors and Actuators A*, **93** (2001) 63.
26. V. A. KAGAN, R. G. BRAY and W. P. KUHN, *Journal of Reinforced Plastics and Composites*, **21**, no. 12 (2002) 1101.
27. V. A. KAGAN and G. P. PINHO, *Journal of Reinforced Plastics and Composites*, **23**, no. 1 (2004) 95.
28. P. A. HILTON, I. A. JONES and Y. KENNISH, *in Proceedings of SPIE—The International Society for Optical Engineering*, **4831** (2002) 44.
29. M. LU, Z. QIAN, W. REN, S. LIU and D. SHANGGUAN, *International Journal of Solids and Structures*, **36**, issue 1 (1999) 65.
30. ABAQUS User's Manual, Version 6.2, Hibbit, Karlsson and Sorensen, USA.